Nonlinear Aeroelastic Scaling Studies of High Aspect-Ratio Wings

Mónica Lima Coelho
amonicalimacoelho@gmail.com

Instituto Superior Técnico, Universidade de Lisboa, Lisboa, Portugal

November 2016

Abstract

In order to improve aircraft range through the reduction of fuel consumptions, the wings aspect-ratio (AR) has been increased. For experimental tests, the scaled model must replicate the desired scaled aeroelastic response of the full-size wing and so, aeroelastic scaling methodologies must be developed. The effects of the chosen primary quantities and of the modal matching approach are analysed using two modal matching approaches (direct modal matching and the Coordinate Modal Assurance Criterion, COMAC) and two scaling methodologies (mass and stiffness distribution matched simultaneously and sequentially), and the option of using a laminated composite beam for the reduced model is analysed. A scaling procedure was applied to a more complex wing model based on the EU FP7 Project NOVEMOR reference wing. Not all sets of primary quantities are usefull. For simple models, sequential matching of stiffness and mass distributions did not provide good results. It was possible to properly scale a simple full-size wing model to a reduced model with laminated composite material. The difference in the approaches for matching the mode shapes is not significant. For a more complex wing, good results were obtained.

Keywords: Modes Matching, Coordinate Modal Assurance Criterion, Composite Materials, Primary Quantities.

1. Introduction

High aspect-ratio wings have been studied with the objective of improving aircraft performance. The wingtip of these wings has less area, which causes less vortex induced downwash, leading to less induced drag. The total drag coefficient, C_D, can be defined as the sum of profile drag coefficient, C_{D_0}, and induced drag coefficient, C_{D_i} [1]:

$$C_D = C_{D_0} + C_{D_i} = C_{D_0} + \frac{{C_L}^2}{\pi e AR}, \qquad (1)$$

where C_L is the lift coefficient, e is the span efficiency factor, and AR is the aspect-ratio.

These wings produce less drag, hence reducing fuel consumptions, and producing more lift providing a higher lift-to-drag ratio, thus resulting in increased endurance [2]. Combining high aspect-ratio and low structural weight results in very flexible wings that can suffer large deformations, leading to geometrical nonlinear behaviour and aeroelastic problems [3]. Because of that, the necessity to study these aeroelastic problems in order to prevent catastrophic structural failure due to aeroelastic phenomena, such as divergence or flutter, increases. In the development of these type of wings, the engineers must guarantee that these phenomena will not occur for any condition within the vehicle's flight envelope. To reduce the costs and time of experimental tests, aeroelastic scaling is used. Its objective is to design a smaller, simpler, thus cheaper and easier to manufacture, wing structure model that can replicate the scaled aeroelastic response of the more complex full wing structure. With this being said, the development of accurate aeroelastic scaling methodologies is very important.

1.1. Topic Overview and State of the Art

All scaling methodologies derive from the non-dimensionalization of the system's governing Equations Of Motion (EOM) according to Buckingham's Π-theorem, which states that if there is a physical situation that can be represented by means of an equation involving a certain number n of physical variables S, then the original equation can be rewritten in terms of a set of dimensionless parameters Π_1,Π_2, ..., Π_{n-m} that are the $n-m$ independent products of the arguments S_1, ..., S_n [4]. The advantage of using dimensionless variables is that the problem is expressed in terms of the minimum number of variables, and the dimensionless equation

of motion is completely unaffected by scale effects, so the values of the dimensionless variables must be the same for both the full-size and scaled models.

The first similarity laws for aeroelastic scaling were defined by Bisplinghoff *et al.* [5], in the 60's, according to whom the three fundamental airplane properties for designing aeroelastic models are the distribution of structural stiffness, external shape, and the distribution of mass. Since then some authors have been developing, analysing and improving different aeroelastic scaling methodologies [2, 3, 6, 7].

1.2. Composite Materials in Aeroelasticity

In order to improve the stiffness of wings, while still keeping low structural weight, composite materials are a good option, and have been widely used in the aircraft industry for many years. The properties of laminated composite materials can have an effect on the aeroelastic behaviour of high-aspect-ratio wings, and are being used to tailor and optimize these wings. The effects that the laminate configuration has on the flutter and divergence speeds was analysed [8, 9, 10].

With this in mind, composite materials can also be a good option for scaled models, simplifying even more the inner structure but still maintaining the same aeroelastic behaviour as the full-scale model.

2. Background

2.1. Aeroelastic Scaling

2.1.1 Equations of Motion

For the EOM, a simplified physics model was chosen: the small disturbance, linear potential partial differential equations (PDE) [11]:

$$[M]\{\ddot{x}\} + [k]\{x\} = [A_k]\{x\} + [A_c]\{\dot{x}\} + [A_m]\{\ddot{x}\} + [M]\{a_g\}, \quad (2)$$

where $\{x\}$ is the vector of elastic degrees of freedom; $[k]$ is the stiffness matrix; $[M]$ is the mass matrix; $[A_i]$ are the aerodynamic terms; and $\{a_g\}$ is the vector of gravitational terms for the corresponding degrees of freedom.

When the EOM describing this system are non-dimensionalized, they yield a set of parameters that are used for scaling the baseline aircraft [11].

2.1.2 Scaling Factors

The selection of scaling factors is critical in any aeroelastic scaling model design, and must be the first step [3]. These scaling factors derive from the non-dimensional parameters of the EOM that represents the physical problem as mentioned before. The parameters to be matched are those that are free after constraints are applied to the model up to the number of primary dimensions involved in the governing equations. For aeroelastic models the primary dimensions are: length (l), time (T), and mass (m) [6]. Based on the primary dimensions, a set of primary quantities, that contain the primary dimensions, must be selected. These primary quantities will be freely chosen and will define the rest of the scaling factors.

The scaling factors needed for the analysis of an aeroelastic scaled model are: length (k_l), time (k_T), frequency (k_f), mass (k_m), air density (k_ρ), velocity (k_V), force (k_F), and inertia (k_I).

2.1.3 Parameters to Match

To properly aeroelastically scale a full-size wing four similarity criteria must be met, plus a fifth similarity for cases where the gravity plays an important role: geometrical similarity; dynamic similarity (mass and stiffness similarity); aerodynamic similarity; and Froude number similarity [3]. To accomplish the similarity of the previous criteria, the following parameters similarity should be achieved [7]: Mach number (M); Reynolds number (Re); Froude number (Fr); External geometry; Frequencies (f) and mode shapes (φ); and Reduced frequencies (κ).

Mach number can be difficult and dispendious to match in wind-tunnel testing and it is usually ignored. For low-speed flying wings that are very flexible, the flow is incompressible, so there should be an attempt of matching the Reynolds number (or at least get it close to match) [12]. Froude number is very important for highly flexible structures, where the inertial forces (gravity loads) have a huge contribution [3].

2.2. Composite Materials

For the composite materials, the mass and stiffness matrix are obtained, first for each ply, recurring to the rule of mixtures. Then, through transformation matrices, the global mass and stiffness matrices are obtained.

2.2.1 Hybrid Composites

Hybrid composites are materials made by combining two or more different types of fibres in a common matrix. They offer a range of properties that cannot be obtained with a single kind of reinforcement [13]. Their behaviour is a weighed sum of the individual components in which there is a more favourable balance between the inherent advantages and disadvantages. As a consequence, a balance in cost and performance can be achieved through proper material design.

3. Scaling Methodologies

Two methodologies will be used: methodology 1 performs the optimization of mass and stiffness dis-

tribution simultaneously while methodology 2 will first match the stiffness distribution and then the mass distribution. These methodologies are defined based on the parameters for which similarity must be met, which are listed previously.

The optimization function used in both methodologies is *fmincon* from Matlab^{TM}. This function finds the minimum of a constrained nonlinear multivariable function. The algorithm chosen was the Sequential Quadratic Programming (SQP) where the function tolerance is defined as 1×10^{-8}.

3.1. Methodology 1

Optimization algorithm for Methodology 1 is represented in Figure 1. The input values include the initial DV's (Design Variables) and the results obtained for the modal analysis of the full-size wing model.

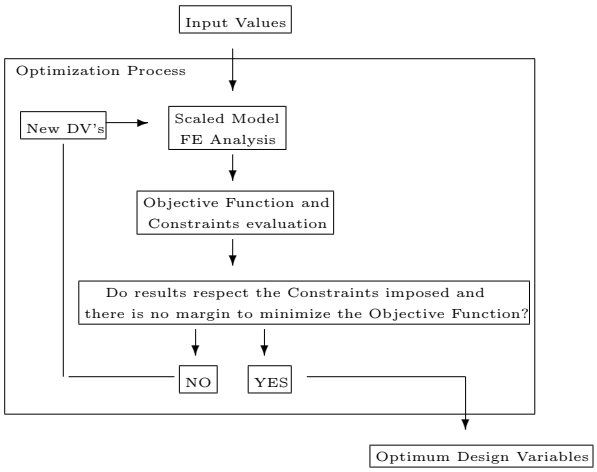

Figure 1: Scaling methodology algorithm 1.

For the frequencies similarity, the absolute value of the difference between the target frequency and the model frequency is used:

$$f_{freq} = \sum_{i=1}^{N} |f_{i_m} - f_{i_t}|, \tag{3}$$

where N is the number of modes, f_{i_m} is the scaled model frequency of mode i and f_{i_t} is the target frequency of mode i.

For the mode shapes two methods are analysed: Coordinate Modal Assurance Criterion (COMAC), and direct modal matching. The COMAC is calculated over a set of mode pairs: analytical versus analytical; experimental versus experimental; or experimental versus analytical. The two modal vectors in each mode pair represent the same modal vector, but the set of mode pairs represents all modes of interest in a given frequency range. For two sets of modes that are to be compared, there will be a value of COMAC computed for each (measurement) degree-of-freedom [14].

$$\text{COMAC} = \frac{|\ \varphi_m^T \times \varphi_t\ |^2}{(\varphi_m^T \times \varphi_m)(\varphi_t^T \times \varphi_t)}, \tag{4}$$

where φ_m corresponds to the mode shapes of the reduced scale model and φ_t to the target mode shapes.

To guarantee that the mode shapes match, COMAC has to result in an identity matrix $N \times N$, being N the number of modes. To accomplish that, the objective function is:

$$f_{\text{COMAC}} = |\sum_{i=1}^{N}(\text{COMAC}(i,i) - 1) + \sum_{i=1, i\neq j}^{N}\sum_{j=1, j\neq i}^{N} \text{COMAC}(i,j)| \tag{5}$$

For the direct mode matching the function is:

$$f_\varphi = |\varphi_m - \varphi_t| \tag{6}$$

The number of modes to match was defined as 5 for both the frequencies and mode shapes.

Finally, the objective function consists in the sum of the functions defined above:

$$ObjFun_1 = f_{freq} + f_{\text{COMAC}}, \tag{7}$$

or:

$$ObjFun_2 = f_{freq} + f_\varphi \tag{8}$$

For the nonlinear constraints the difference between the dynamic frequencies is considered. The tolerance considered is of 5 %. The Root Mean Square (RMS) is used, and so the constraints are:

$$c \leq \left(\sqrt{\frac{1}{N}\sum_{1}^{N}(f_{i_m} - f_{i_t})^2} - 0.05 \right), \tag{9}$$

3.2. Methodology 2

In this methodology, the stiffness and mass distribution are matched sequentially. First, the stiffness distribution is matched by matching the deformation of the reduced model with the scaled deformation of the full-size wing, optimizing the dimensions of the section of the reduced model. Then, the mass distribution similarity is met by matching the frequencies and mode shapes, which is accomplished by adding mass points to the model. The optimization algorithm for methodology 2 is presented in Figure 2.

Optimization Process 1

$$f = \sum_{i=1}^{NN}(u_{i_m} - u_{i_t}), \tag{10}$$

where NN is the number of nodes, u_{i_m} is the deformation of the reduced model for node i, and u_{i_t} is the target deformation for node i.

The constraint imposed to optimization process 1 is that the RMS of the deformation should be less than 5%:

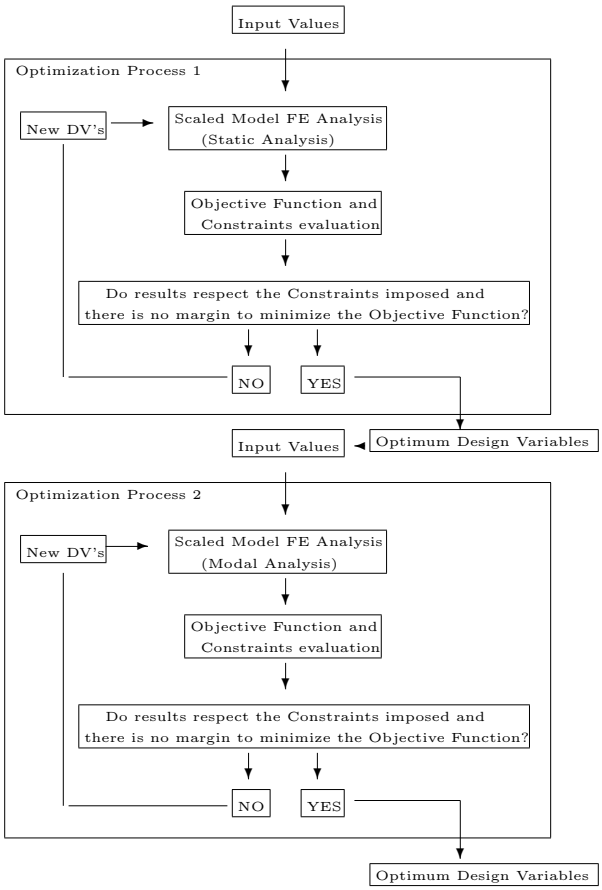

Figure 2: Scaling methodology algorithm 2.

$$c \leq \left(\sqrt{\frac{1}{NN} \sum_{1}^{NN} (u_{i_m} - u_{i_t})^2} - 0.05 \right), \qquad (11)$$

Optimization Process 2

For the frequencies similarity, the absolute value of the difference between the target frequency and the model frequency is used, the same used in methodology 1. To match the mode shapes, we resort to the Coordinate Modal Assurance Criterion (COMAC), since this method has proven to provide better results (see Section 4.6). Therefore the objective function is the one presented in Equation 7.

For the nonlinear constraints, the same option described in methodology 1 is considered, which corresponds to Equation 9.

4. Primary Quantities

The choice of the primary quantities can be influenced by different aspects based on the type of experimental test that the model is intended for. With the objective of analysing the influence of the primary quantities choice in the scaling procedure, five different sets will be defined and applied to a simple model, and are given in Table 2.

4.1. Full-Size Wing

The full-size wing consists of a rectangular wing made of aluminium. In order to simplify the problem, the wingbox is a rectangular box beam represented in Figure 3. The dimensions, material properties, and conditions of flight are presented in Table 1.

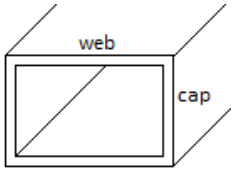

Figure 3: Full-size wing simplified wingbox.

Table 1: Full size wing dimensions, material properties, and flight condition.

Span (m)	20
Chord (m)	1
Web thickness (m)	0.01
Web length (m)	0.3
Cap thickness (m)	0.01
Cap length (m)	0.2
Material density (kg/m^3)	2700
Young's Modulus (GPa)	70
Shear Modulus (GPa)	26
Velocity (m/s)	40
Altitude (m)	0
Air density (kg/m^3)	1.225
Air kinematic viscosity (m^2/s)	1.46×10^{-5}

4.2. Scaled Model

For the inner structure of the scaled model two different wingbox sections were tested for each set: the same section as the full-size model (section 1), and a rectangular beam section (section 2). The DV's for section 1 are the caps and webs thicknesses (tw and tc, respectively) and lengths (w and c, respectively), and for section 2 the DVs are the height and length (w and c respectively). The DVs are represented in Figure 4.

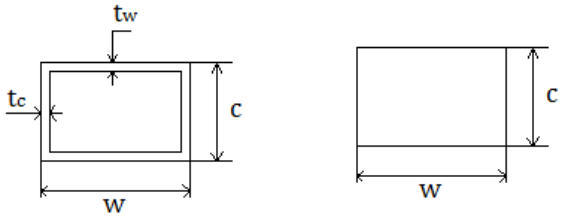

(a) Section 1 DV's (b) Section 2 DV's

Figure 4: DV's for the two sections.

The material of the scaled model is also aluminium with the same properties as the full-size wing model, described in Table 1.

4.3. Scaling Factors

Based on the SI units of each parameter, the scaling factors are defined combining the ratios of the

primary quantities. The velocity scaling factor for Sets 1 and 2 is defined based on the Froude number similarity despite being a primary quantity for Set 1; for Sets 3 and 5 the velocity is defined based on the lift coefficient CL, considering that the trim condition of the full-size wing should be the same as the reduced model; for Set 4 the velocity is defined as a primary quantity.

Table 2: Scaling factors for the five different sets of primary quantities.

	Scaling Factors				
	Set 1	**Set 2**	**Set 3**	**Set 4**	**Set 5**
	ρ, V, b	ν, b, ρ	f, M, b	ν, ρ, V	p, b, ρ
k_l	$\frac{b_m}{b_w}$	$\sqrt[3]{k_\nu^2}$	$\frac{b_m}{b_w}$	$\frac{k_\nu}{k_V}$	$\frac{b_m}{b_w}$
k_T	$\frac{k_l}{k_V}$	$\frac{k_l^2}{k_\nu}$	$\frac{1}{k_f}$	$\frac{k_\nu}{k_V^2}$	$\sqrt{\frac{k_\rho k_l^2}{k_p}}$
k_f	$\frac{k_V}{k_l}$	$\frac{k_\nu}{k_l^2}$	$\frac{f_m}{f_w}$	$\frac{k_V^2}{k_\nu}$	$\sqrt{\frac{k_p}{k_\rho k_l^2}}$
k_M	$k_\rho k_l^3$	$k_\rho k_l^3$	$\frac{M_m}{M_w}$	$\frac{k_\nu^3 k_\rho}{k_V^3}$	$k_\rho k_l^3$
k_ρ	$\frac{\rho_m}{\rho_w}$	$\frac{\rho_m}{\rho_w}$	$\frac{k_M}{k_l^3}$	$\frac{\rho_m}{\rho_w}$	$\frac{\rho_m}{\rho_w}$
k_V	$\sqrt{k_l}$	$\sqrt{k_l}$	$k_f k_l$	$\frac{V_m}{V_w}$	$\sqrt{\frac{k_p}{k_\rho}}$
k_F	$k_\rho k_V^2 k_l^2$	$k_\rho k_\nu^2$	$k_M k_l k_f^2$	$k_\rho k_\nu^2$	$k_p k_l^2$
k_I	$k_\rho k_l^5$	$k_\rho k_l^5$	$k_M k_l^2$	$\frac{k_\nu^5}{k_\rho} k_V^5$	$k_\rho k_l^5$

The analyses will be made only for wind-tunnel tests. The initial values chosen for the primary quantities of the scaled model for sets 1, 3 and 5 are listed in Table 3.

Table 3: Primary quantities values and the Sets where each primary quantity is applied.

	Wind-Tunnel Test	Sets
ρ_m (kg/m^3)	1.225	1, 5
b_m (m)	2	1, 3, 5
f_m (Hz)	Full-size wing frequencies	3
m_m (kg)	1	3
p_m (GPa)	70	5

For Sets 2 and 4, the kinematic viscosity and density of the air are defined together. The kinematic viscosity ratio should be smaller than the velocity ratio to obtain a small span for the reduced model. Considering an altitude of 0 m for both the reduced and the full-size wing, the kinematic viscosity ratio will be 1. For Set 2, since the velocity is limited by the similarity of the trim condition, the length scaling factor can only be altered by changing the kinematic viscosity scaling factor. For the flight condition defined for the full-size wing there is no viable solution, and this set cannot be used, so we assume, for Set 2 only, a different flight condition for the full-size wing, which is presented in Table 4. For Set 4 it is possible to select the reduced model velocity, and therefore to obtain a velocity scaling factor higher than 1 in order to have a reduced length scaling factor. The altitude chosen for the scaled model of both sets is 0 m and the primary quantities values for this altitude are presented in Table 4.

Using the values chosen for the primary quantities the scaling factors can be obtained and are listed in Table 5.

Table 4: Flight condition of the full-size wing and primary quantities values for Sets 2 and 4.

Flight condition of the full-size wing	V (m/s)	40
	h (m)	15000
	ρ (kg/m^3)	0.1948
	ν (m^2/s)	7.30×10^{-5}
Primary quantities values	ρ (kg/m^3)	1.225
	ν (m^2/s)	1.46×10^{-5}
	V for Set 4 (m/s)	100

Table 5: Scaling factors for the five different sets of primary quantities.

	Scaling Factors				
	Set 1	**Set 2**	**Set 3**	**Set 4**	**Set 5**
	ρ, V, b	ν, b, ρ	f, M, b	ν, ρ, V	p, b, ρ
k_l	0.1000	0.3420	0.1000	0.4000	0.1000
k_T	0.3162	0.5848	1	0.1600	0.1000
k_f	3.1623	1.7100	1	6.2500	10
k_M	0.0010	0.2515	0.0039	0.0640	0.0010
k_ρ	1	6.2885	3.8580	1	1
k_V	0.3162	0.5848	0.1000	2.5000	1
k_F	0.0010	0.2515	3.8580×10^{-4}	1	0.0100
k_I	1×10^{-5}	0.0294	3.8580×10^{-5}	0.4000	1×10^{-5}

4.4. Methodology

Methodology 1 will be used for all sets. For the constraints function the natural frequencies are used, which is defined in Equation 9. For the modes matching, the two approaches will be used and compared using section 2 only. In order to analyse the difference in the methodologies described, both methodologies will be used with Set 1.

4.5. Results

The results were obtained for all sets of primary quantities for section 1 and section 2, using COMAC. When considering Set 4 of primary quantities, the optimization process was unable to obtain a feasible solution that respected the constraints imposed using both sections.

The final dimensions, material properties and condition of flight of the reduced model for each set of primary quantities are presented in Table 6. Also the best overall result of the objective function value and number of function calls is listed.

Table 6: Final dimensions and best overall result for each set using COMAC.

	Set 1	Set 2	Set 3	Set 5
w	0.01228	0.07769	0.00388	0.03000
c	0.00894	0.05653	0.00283	0.02000
t_w	-	-	-	0.00100
t_c	-	-	-	0.00100
b	2	6.83990	2	2
ρ	2700	2700	2700	2700
E	70	70	70	70
m	0.25920	0.25920	1	0.25920
ρ_{air}	1.22500	1.22500	4.72605	1.22500
ν_{air}	1.46×10^{-5}	1.46×10^{-5}	4.6169×10^{-7}	1.46×10^{-5}
U	12.64910	23.39200	4	40
fval	0.03831	0.01809	0.02942	0.02149
fcount	985	1017	973	781

Analysing the different primary quantity sets one

can see that for this simple case, it is possible to obtain an approximately similar value for the objective function with all sets. Considering the number of function calls, and comparing the best results for each set, there are no major differences. This means that all sets are plausible to be chosen, depending on the goal and type of experimental test.

However, Set 2 is restrained by the flight condition of the full-size wing for wind-tunnel tests, and by the dimensions of the tunnel, and Set 3 resulted in air properties that do not correspond to any of the properties that are encountered in nature, at any height.

4.6. Modal Matching Approach Analysis

To evaluate which approach is better, we started by obtaining the optimum design variables with all decimal places for both approaches. Then, both optimum design variables (obtained with direct modal matching and COMAC) are used as initial point for the COMAC modal matching approach, and the first objective function value registered. Also, a modal analysis was made to the reduced model using the DV's obtained with each approach. By analysing the results obtained it was possible to conclude that the COMAC modal matching approach is better for all sets.

4.7. Reynolds Matching Analysis

With the objective of evaluating whether Reynolds number similarity is met, XFOIL$^{\text{TM}}$is used. Reynolds and Mach numbers are calculated for the full-size wing and for the scaled model of each set. Then, XFOIL$^{\text{TM}}$is used to evaluate if there are major differences in the curve L/D.

For Set 3, since the air conditions are not encountered naturally at any height, the temperature was calculated based on the perfect gas rule:

$$T = \frac{p}{R\rho}, \tag{12}$$

where p is the pressure of the air, considered to be 1 atm, R is the specific gas constant (287.058 J/kgK), and ρ is the density of the air obtained for this reduced model. The final temperature value is lower than the condensation temperature for air. Therefore, we will consider the temperature of 123.15 K as an approximation, for which the density and kinematic viscosity are 2.793 kg/m^3 and 3.08×10^{-6} m^2/s, respectively.

The curves L/D for all sets and correspondent full-size wing are represented in Figure 5.

It is possible to see that for Set 2, for which the scaling factors were defined based on the attempt of matching the Reynolds number, the curves of the reduced models match the one of the full-size wing. For Sets 1, 3 and 5 the smaller Reynolds number causes the viscosity in the air to increase, leading to higher values of drag.

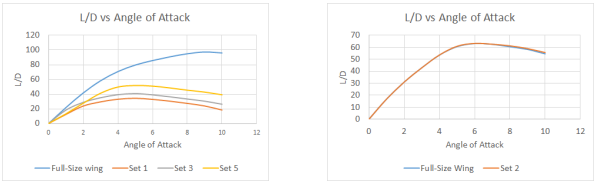

(a) L/D curves for Sets 1, 3, and 5, and the correspondent full-size wing

(b) L/D curves for Set 2, and the correspondent full-size wing

Figure 5: L/D curves for all sets and the correspondent full-size wing.

4.8. Methodologies Analysis

In order to compare which methodology is better, Methodology 2 was used considering Set 1 of primary quantities. Although proven well developed by recurring to Set 5, for which the final solution is known, Methodology 2 was not able to properly scale the full-size wing using Set 1. This is due to the fact that the material of the model is not well scaled (in Set 5, this does not happen since the scaling factors are calculated based on the matching of material properties), meaning that the deformation matching does not necessarily result in proper modal matching, and adding different masses to a beam do not alter the modal response to the extend needed.

5. Laminated Composite Material Scaled Model

To verify if it is possible to obtain a reduced model made of laminated composite material that can replicate the scaled aeroelastic response of the full-size model, a different scaling procedure was developed.

5.1. Full-size Wing

The full-size wing used for this scaling analysis is the same used in the primary quantities analysis, which is described in Section 4.1.

5.2. Scaled Model

For the reduced model, a symmetric laminate with a rectangular cross-section and 5 laminas is used. In order to obtain a better value, hybrid composites are considered. The structural performance of the resulting composite material will not be analysed, which means that the material might not be properly designed. The matrix material considered is Epoxy, for which material properties are listed in Table 7. For the fibre materials, 4 options are provided and listed in the same Table.

Table 7: Fibre and Epoxy material properties.

	E_f (GPa)	ρ_f (kg/m^3)	υ_f
Epoxy	4.5	1200	0.4
E-Glass Fibre	72	2550	0.21
S-Glass Fibre	86	2485	0.21
Kevlar 49	112	1450	0.36
Carbon IM7	300	1790	0.35

5.3. Methodology

Set 1 of primary quantities is used, and the scaling factors will also be the same and are listed in Table 5.

Methodology 1 is used considering both approaches for matching the modal response. The constraints used are the ones described by Equation 9, in which natural frequencies are used. The algorithm is represented in Figure 6.

On a first optimization process, the DV's are: the thicknesses of the plies (t_i); the fraction of fibre in each ply (V_{f_i}); the orientation of the fibres in each ply (O_{r_i}); the length of the cross section (b); the fibre Young's Modulus of each ply (E_{f_i}); the fibre density of each ply (ρ_{f_i}); and the Poisson Coefficient of each ply (υ_{f_i}). Since the laminate is symmetric, DV's only need to be defined for plies 2, 1, and 0.

In order to guarantee that the fibre material properties correspond to a real material, the results are compared with the 4 options, listed in Table 7. The material that provides the closest material properties values is selected.

Finally, a second optimization process is performed with the fibre materials defined, and not as DV's.

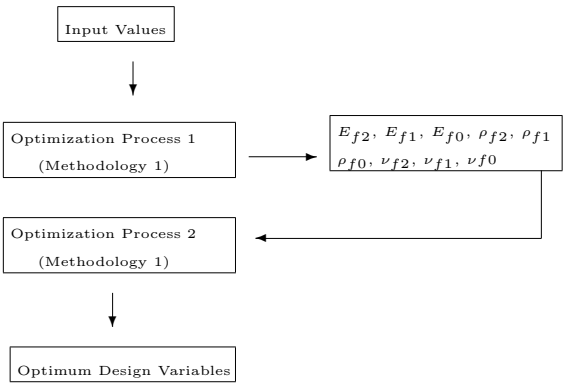

Figure 6: Scaling methodology algorithm for the analysis of a scaled model made of laminated composite materials.

Since there are some limitations in the characteristics of a laminated composite material, boundaries for the DV's correspondent to these characteristics were defined and are presented in Table 8.

Table 8: Fibre DV's boundaries.

DV's	Upper Boundary	Lower Boundary
V_{f_i}	70	50
O_{r_i} (rad)	$\pi/2$	$-\pi/2$
E_{f_i} (GPa)	300	70
ρ_{f_i} (kg/m$^)$	2600	1000
υ_{f_i}	0.4	0.1

5.4. Results

The results obtained for the optimization of a reduced model made of hybrid composite materials resulted in a minimum objective function value and number of function calls of 0.1521 and 7392, respectively, for the complete optimization process using COMAC, and 0.2399 and 4040 for direct modal matching. Comparing the frequencies obtained for the reduced model using both approaches, we concluded that the results are better using direct modal matching.

Despite the higher value of the final objective function in comparison with the previous results, the scaling procedure was able to properly scale the full-size wing to a reduced model made of hybrid composite materials. Also the number of function calls is much higher when compared to a metallic reduced model due to the fact that there are more design variables involved.

6. Complex Wing

A scaling procedure is applied to a more complex wing based on the NOVEMOR project of the EU FP7 reference wing, which was stretched to have a higher aspect-ratio, 16. The geometry of the new wing is illustrated in Figure 7 and its main characteristics are listed in Table 9.

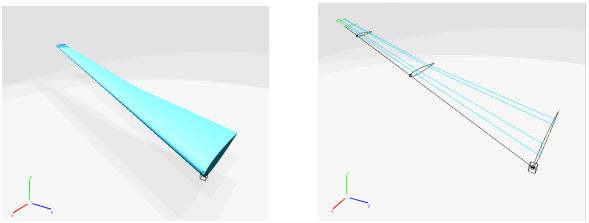

(a) Geometric shape (b) Structural layout

Figure 7: Complex wing model geometric shape and structural layout.

Table 9: Geometric characteristics of the new wing.

Span b_{new}(m)	41.95
First-half span $b_{1_{new}}$ (m)	8.24
Second-half span $b_{2_{new}}$ (m)	12.73
Mean Aerodynamic Chord $M.A.C._{new}$ (m)	2.62
Root Chord $c_{r_{new}}$ (m)	4.95
Break Chord $c_{b_{new}}$ (m)	2.61
Tip Chord $c_{t_{new}}$ (m)	1.13

The wingbox model depicted in Figure 7 consists of a square shape box, in which the upper and lower layers follow the airfoil shape, instead of being straight. As for the side layers, they consist on the spars of the wing, which are placed at 25% and 75% of the local chord of the airfoil. The material of the wing is aluminium for which properties are presented in Table 1. The skin thicknesses t_s in the upper and lower layers, and is adimensionalized by the maximum thickness of the airfoil. As for the spars thicknesses t_w, they are defined in function of the chord length. Constant spars and skins of 28.0 and 5.6 mm, respectively, were assumed for this model.

The dynamic analysis and scaling procedure are performed considering three flight conditions: cruise, alternate and hold. The angle of attack at which the analyses were computed was defined such that wing lift equals the weight of the aircraft (58 tons). The characteristics of each condition of flight are presented in Table 10. All the analyses conducted for this wing model were done using an in-house nonlinear aeroelastic framework [15]. This computational framework includes: a 3D panel model with compressibility and viscous corrections to model the aerodynamics; a 3D nonlinear condensed beam model for structural modelation; and a loosely-coupled Fluid-Structure Interaction algorithm responsible for computing the aeroelastic response in the time domain.

Table 10: Characteristics of the flight conditions for the full-size wing.

	Cruise	Alternate	Hold
Mach Ma	0.78	0.5	0.3
Altitude h (m)	11582.4	5486.4	609.6
Air density ρ (kg/m^3)	0.3320	0.6981	1.1549
Velocity U (m/s)	230.1546	159.2705	101.3838
Trim lift coefficient $C_{L_{trim}}$	0.5883	0.5841	0.8715
Trim angle of attack α_{trim} (°)	5.3645	5.3267	7.9469

Both full-scale and reduced-scale models were defined considering the same aerodynamic and structural meshes. For the aerodynamic mesh the following distribution was set: 28 spanwise divisions; 40 chordwise divisions; and wake elements with lengths of 100 chords. Regarding the structural mesh, 50 nonlinear beam finite elements equally spaced in the span direction were considered.

6.1. Scaled Model

For the NOVEMOR wing only Sets 1 and 5 were considered for the primary quantities selection. A 1/10th geometric scale was considered for devising the scaled model, which was defined with the same wingbox shape as the full-size wing (see Figure 7). For the reduced model using Set 5 the material is also aluminium, and For Set 1 the material is Nylon, for which properties are listed in Table 11.

Table 11: Geometric characteristics of the new wing.

Young's Modulus (GPa)	1.27
Shear Modulus (GPa)	0.3
Density (kg/m^3)	1010
Yield stress (MPa)	35

6.2. Results

Prior to compare the aeroelastic behaviour of both models, the aerodynamic and structural performance was evaluated. Table 12 shows the differences in C_L, C_D, C_M and natural frequencies between the two models for Set 5. From this table, one can clearly see that the natural frequencies are exactly matched. Regarding the aerodynamic coefficients small differences were found, which are due to the fact that Reynolds number was not matched (accounted for in the implemented aerodynamic model through a viscous drag correction factor).

The nonlinear aeroelastic response in the time domain was computed assuming the wing undeformed at the initial instance and released into a constant airflow, corresponding to each considered flight condition. A very good agreement was found between full and reduced scale models for Set 5 as one noticed in Figure 8, where the aeroelastic response measured at the wing tip in plunge, pitch and chord degrees-of-freedom is shown. The discrepancies found are associated with the viscous effects considering in the computational framework employed for the analyses.

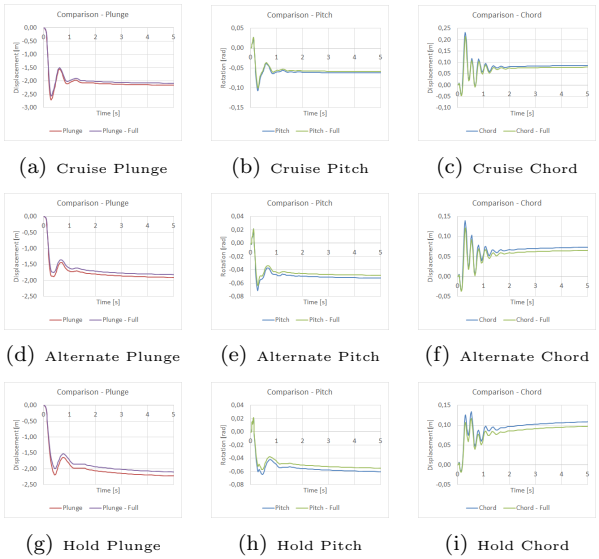

(a) Cruise Plunge (b) Cruise Pitch (c) Cruise Chord

(d) Alternate Plunge (e) Alternate Pitch (f) Alternate Chord

(g) Hold Plunge (h) Hold Pitch (i) Hold Chord

Figure 8: Comparison of the aeroelastic response measured at the wing tip for plunge, pitch and chord degrees-of-freedom for the reduced and full size aircraft for Set 5.

Froude number similarity was not achieved in the scaling process of Set 5: if it is used to define the airspeed for each flight condition, different air loadings are obtained, thus rendering in different aeroelastic responses.

Considering Set 1 the Mach number similarity was not achieved, resulting in a poor matching of the aerodynamic and strutural response for the alternate and hold flight conditions. Therefore, the properties of the air (density and temperature) were altered in order to provide Mach number similarity for these cases. For cruise condition, the air properties did not need to be changed. The results are presented in Table 13 and Figure 9.

By matching Froude number for Set 1, the velocity scaling factor did not have into account the Mach number similarity, resulting in poor matching of aerodynamic and structural responses. This could imply that, despite being considered as

Table 12: Comparison of the aerodynamic and dynamic results between full and reduced models for Set 5.

	Aerodynamics									
	Cruise			Alternate			Hold			
	C_L (-)	C_D (-)	C_M (-)	C_L (-)	C_D (-)	C_M (-)	C_L (-)	C_D (-)	C_M (-)	
Full Scale	0.7792	0.0674	1.3048	0.6972	0.0141	1.0821	0.8711	0.0206	1.3813	
Target	0.7792	0.0674	1.3048	0.6972	0.0141	1.0821	0.8711	0.0206	1.3813	
Reduced Scale	0.7794	0.0660	1.3054	0.6989	0.0132	1.0846	0.8716	0.0195	1.3822	
Difference (%)	0.03	2.12	0.04	0.23	6.06	0.23	0.06	5.34	0.06	
	Natural Frequencies									
	F1 (Hz)	F2 (Hz)	F3 (Hz)	F4 (Hz)	F5 (Hz)	F6 (Hz)	F7 (Hz)	F8 (Hz)	F9 (Hz)	F10 (Hz)
Full Scale	1.2642	5.1286	5.2175	11.634	20.791	21.173	27.663	34.124	47.378	50.094
Target	12.642	51.286	52.175	116.34	207.91	211.73	276.63	341.24	473.78	500.94
Reduced Scale	12.642	51.286	52.175	116.34	207.91	211.73	276.63	341.24	473.78	500.94
Difference (%)	0.00	0.00	0.00	0.00	0.00	0.00	0.00	0.00	0.00	0.00
Mode Shapes	1^{st} Flap	2^{nd} Flap	1^{st} Chord	3^{rd} Flap	2^{nd} Chord	4^{th} Flap	1^{st} Torsion	5^{th} Flap	3^{rd} Chord	6^{th} Flap

Table 13: Comparison of the aerodynamic and dynamic results between full and reduced models for Set 1.

	Aerodynamics									
	Cruise			Alternate			Hold			
	C_L (-)	C_D (-)	C_M (-)	C_L (-)	C_D (-)	C_M (-)	C_L (-)	C_D (-)	C_M (-)	
Full Scale	0.7792	0.0674	1.3048	0.6972	0.0141	1.0821	0.8711	0.0206	1.3813	
Target	0.7792	0.0674	1.3048	0.6972	0.0141	1.0821	0.8711	0.0206	1.3813	
Reduced Scale	0.7799	0.0678	1.3061	0.6977	0.0118	1.0893	0.8717	0.0190	1.3820	
Difference (%)	0.09	0.51	0.10	0.07	16.61	0.67	0.07	8.18	0.05	
	Natural Frequencies									
	F1 (Hz)	F2 (Hz)	F3 (Hz)	F4 (Hz)	F5 (Hz)	F6 (Hz)	F7 (Hz)	F8 (Hz)	F9 (Hz)	F10 (Hz)
Full Scale	1.2642	5.1286	5.2175	11.634	20.791	21.173	27.663	34.124	47.378	50.094
Target	2.7445	11.198	11.357	25.368	45.414	46.080	60.090	74.412	103.31	109.01
Reduced Scale	2.7118	10.584	11.662	23.490	41.826	43.160	52.560	67.103	93.734	96.325
Difference (%)	1.19	5.49	2.69	7.40	70.90	6.34	12.53	9.82	9.27	11.64
Mode Shapes	1^{st} Flap	2^{nd} Flap	1^{st} Chord	3^{rd} Flap	2^{nd} Chord	4^{th} Flap	1^{st} Torsion	5^{th} Flap	3^{rd} Chord	6^{th} Flap

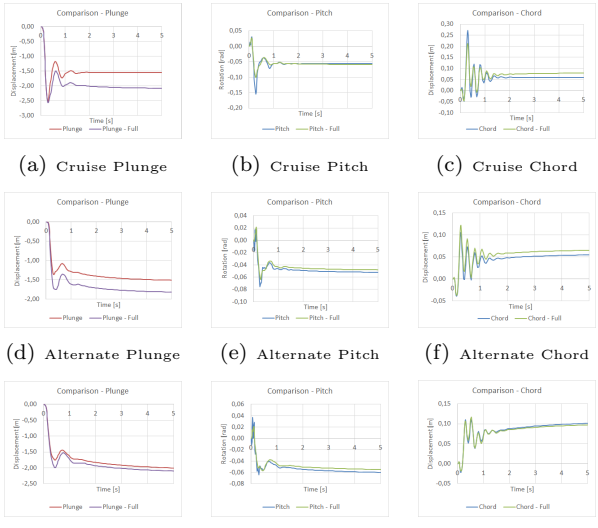

(a) Cruise Plunge (b) Cruise Pitch (c) Cruise Chord

(d) Alternate Plunge (e) Alternate Pitch (f) Alternate Chord

(g) Hold Plunge (h) Hold Pitch (i) Hold Chord

Figure 9: Comparison of the aeroelastic response measured at the wing tip for plunge, pitch and chord degrees-of-freedom for the reduced and full size aircraft for Set 1.

mandatory in aeroelastic scaling, Froude number similarity provides worse results than when Mach number similarity is considered. This also happens for the simplified model analysis when comparing the different sets of primary quantities and the parameters for which each set's velocity scaling factor is defined.

7. Conclusions

The most usable sets of primary quantities are Set 1 and 5, despite the differences in the aerodynamic response for Set 1. Analysing the results, we concluded that Mach number similarity could be more relevant to aeroelastic scaling than Froude number similarity for some applications. For overly simplified models, sequential matching of stiffness and mass distributions does not provide good results.

As for the laminated composite material reduced model, it was possible to properly scale a simple full-size wing model to a reduced model.

Comparing the approaches used to match the modal response of the reduced model to the scaled modal response of the full-size wing, it was not possible to reach a conclusion on which approach is better, since the differences were not significant and also the number of test cases is not sufficient.

For a more complex wing, Set 5 of primary quantities provided good results, despite the non-similarity of the Froude number. As for Set 1 of primary quantities, it was necessary to alter the air properties of the reduced model in order to provide Mach number similarity and match the response of the aircraft in hold and alternate condition of flight.

In future work, Sets 1 and 5 could be further explored in order to try and match the aerodynamic response. Composite materials proved to be a material to have into account for aeroelastic scaled models, despite the difficulties in manufacturing, and

an analysis in more complex structures should be done. Also an analysis of the structural response of the hybrid laminate should be done. Constraints should be added in order to guarantee the manufacturing of the laminate.

References

[1] Ira Herbert Abbott and Albert Edward Von Doenhoff. *Theory of wing sections, including a summary of airfoil data*. Dover Publications Inc., New York, 1959.

[2] C. Spada, F. Afonso, F. Lau, and A. Suleman. Aeroelastic analysis of high aspect-ratio wings. In *54th AIAA Aerospace Sciences Meeting, AIAA Science and Technology Forum and Exposition (SciTech 2016)*, San Diego, California, January 2016.

[3] Zhiqiang Wan and Carlos ES Cesnik. Geometrically nonlinear aeroelastic scaling for very flexible aircraft. *AIAA Journal*, 52(10):2251–2260, Jul 2014.

[4] E. Buckingham. On physically similar systems; illustrations of the use of dimensional equations. *Phys. Rev.*, 4:345–376, Oct 1914.

[5] Raymond L Bisplinghoff, Holt Ashley, and Robert L Halfman. *Aeroelasticity*. Dover Publications, Inc., 31 East 2nd Street, Mineola, N.Y. 11501, 1996.

[6] Maxwell Blair, Daniel Garmann, R Canfield, V Bond, Pedro Pereira, and Afzal Suleman. Non-linear aeroelastic scaling of a joined-wing concept. In *48th AIAA/ASME/ASCE/AHS/ASC Structures, Structural Dynamics, and Materials Conference*, volume 1887, Honolulu, Hawaii, April 2007.

[7] Anthony P Ricciardi, Robert A Canfield, Mayuresh J Patil, and Ned Lindsley. Nonlinear aeroelastic scaling of a joined-wing aircraft. In *53rd AIAA/ASME/ASCE/AHS/ASC structures, structural dynamics and materials conference, AIAA*, volume 1454, Honolulu, Hawaii, April 2012.

[8] Carlos ES Cesnik, Dewey H Hodges, and Mayuresh J Patil. Aeroelastic analysis of composite wings. In *Proceedings of the 37th Structures, Structural Dynamics, and Materials Conference*, Salt Lake City, UT, U.S.A, April 1996.

[9] Masaki Kameyama and Hisao Fukunaga. Optimum design of composite plate wings for aeroelastic characteristics using lamination parameters. *Computers and Structures*, 85(3):213–224, 2007.

[10] Olivia Stodieck, Jonathan E Cooper, Paul M Weaver, and Paul Kealy. Improved aeroelastic tailoring using tow-steered composites. *Composite Structures*, 106:703–715, 2013.

[11] Jenner Richards. *An Experimental Investigation of a Joined Wing Aircraft Configuration Using Flexible, Reduced Scale Flight Test Vehicles*. PhD thesis, University of Victoria, 2014.

[12] Carlos E. Cesnik. Workshop on nonlinear aeroelasticity and flight dynamics of very flexible aircraft.

[13] MS Sreekala, Jayamol George, MG Kumaran, and Sabu Thomas. The mechanical performance of hybrid phenol-formaldehyde-based composites reinforced with glass and oil palm fibres. *Composites science and technology*, 62(3):339–353, 2002.

[14] Randall J Allemang. The modal assurance criterion–twenty years of use and abuse. *Sound and vibration*, 37(8):14–23, 2003.

[15] A. Suleman, F. Afonso, J. Vale, . Oliveira, and F. Lau. Non-linear aeroelastic analysis in the time domain of high-aspect-ratio wings: Effect of chord and taper-ratio variation. *The Aeronautical Journal*, 2016.